

Wind reversals in turbulent Rayleigh-Bénard convection

F. Fontenele Araujo¹, Siegfried Grossmann², and Detlef Lohse¹

¹Department of Applied Physics and J. M. Burgers Centre for Fluid Dynamics,
University of Twente, 7500 AE Enschede, The Netherlands

²Department of Physics, University of Marburg, Renthof 6, D-3502 Marburg, Germany

(Dated: December 2, 2024)

The phenomenon of abrupt and irregular reversals of the large-scale circulation in turbulent Rayleigh-Bénard convection is theoretically analysed. The force and thermal balance on a single plume parcel detached from the thermal boundary layer yields a set of coupled nonlinear equations, whose dynamics is related to the Lorenz equations. For Prandtl and Rayleigh numbers in the range $3 \leq \text{Pr} \leq 1000$ and $10^7 \leq \text{Ra} \leq 10^{14}$, the model shows: (i) chaotic reversals may be exhibited at $\text{Ra} \geq 10^8$; (ii) the Reynolds number based on the root mean square velocity scales as $\text{Re}_{rms} \sim \text{Pr}^{-(0.80 \pm 0.01)} \text{Ra}^{0.43 \pm 0.01}$; and (iii) the mean reversal frequency follows effective scaling laws $\omega/(\nu L^{-2}) \sim \text{Ra}^{0.44} - \text{Ra}^{0.52}$ with decreasing Pr and $\omega/(\nu L^{-2}) \sim \text{Pr}^{-0.83} - \text{Pr}^{-0.95}$ with increasing Ra . The phase diagram of the model is sketched, and the observed transitions are discussed.

One important issue in turbulent Rayleigh-Bénard convection is the interplay between the large-scale circulation (the so-called wind) [1] and the dynamics of plumes detached from the thermal boundary layers [2]. In particular, such interplay seems to be relevant in the process of circulation reversals, which occur in an irregular time sequence [3, 4]. Remarkably, similar reversals are also observed in the wind direction of the atmosphere [5] and in the magnetic polarity of the earth [6].

Theoretically, the phenomenon of wind reversals in turbulent Rayleigh-Bénard convection is still poorly understood, but at least its qualitative mechanism can be described as follows [7]: If an uprising hot plume gets too fast because of the temperature surplus, it fails to cool down sufficiently when passing the top plate. It then is still warmer than the ambient fluid when advected down along the side wall. By buoyancy it therefore loses speed and counteracts the large-scale circulation. Indeed the downward wind may be counteracted so strongly that it stops or even reverses its direction. This mechanism can be effective only for sufficiently strong wind, i.e., for sufficiently large Reynolds number, because for slow motion the thermal diffusivity κ has enough time to reduce the temperature surplus of the originally warmer plume parcel relative to its neighbourhood. Then its power to reverse the circulation by buoyancy is gone. The present Letter aims to make the above picture more quantitative by means of a deterministic dynamical system, which mimics the basic equations of thermal convection.

The model: Consider a spherical plume parcel of radius ℓ , describing a circular motion, as shown in figure 1. Supposing that the parcel velocity U is a function of time only (with the surrounding fluid at rest), it is reasonable to expect that its dynamics is essentially a matter of balance between buoyancy and drag.

In the Boussinesq approximation the buoyancy force (per volume) is given by $\mathbf{f}_b = -\rho_0 \alpha_p (T - T_0) \mathbf{g}$, where ρ_0 is a reference density, α_p the isobaric thermal expansion coefficient, T the plume temperature, T_0 a reference

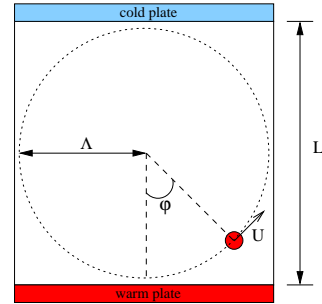


FIG. 1: Sketch of the motion of a single plume parcel in an aspect-ratio-one container. The circulation radius $\Lambda = L/2$.

temperature, and g the gravitational acceleration. On the other hand, the drag force (per volume) on the plume parcel has a strength $f_d = \frac{3}{8} \rho_0 C_\varepsilon(\text{Re}) U^2 \ell^{-1}$, where $C_\varepsilon(\text{Re})$ is the drag coefficient, and the Reynolds number is defined by $\text{Re} = L U \nu^{-1}$.

To further characterize ℓ and C_ε , two assumptions are made: (i) Since the turbulent regime is characterized by an eddy structure, we express ℓ in terms of the Kolmogorov length scale η , namely $\ell \simeq 10 \eta$, where the prefactor corresponds to the crossover between the dissipation and the inertial subranges [8]; and (ii) for the drag coefficient we adopt a mean-field type theory [9]

$$C_\varepsilon(\text{Re}) = \sqrt{\left(\frac{6}{b}\right)^3 \left[\sqrt{\frac{3b^3}{8} \frac{1}{\text{Re}}} + \sqrt{1 + \frac{3b^3}{8 \text{Re}^2}} \right]}, \quad (1)$$

where $b = 8.4$ is the Kolmogorov constant. Equation (1) describes the transition from drag in the viscous regime to drag in the turbulent regime. As pointed out in reference [9], it well agrees with experimental data. Under such assumptions, the length scale ℓ can be written in terms of Re as:

$$\ell \simeq 10 L [C_\varepsilon(\text{Re})]^{-1/4} \text{Re}^{-3/4}. \quad (2)$$

Now, let us consider the thermal interaction between the plume parcel and its surrounding. Strictly speaking, the surrounding consists of the fluid as well as the sidewalls, and the top and bottom plates. We do not distinguish between all these and describe the temperature of the surrounding $T_s(\varphi)$ by a time-independent profile:

$$T_s(\varphi) = T_0 + \frac{\Delta}{2} \cos \varphi, \quad (3)$$

where Δ is the temperature difference between the horizontal plates. We Fourier expand the temperature variable of the plume parcel:

$$T(\varphi, t) = T_0 + \sum_{n=1}^{\infty} [A_n(t) \sin(n\varphi) + B_n(t) \cos(n\varphi)], \quad (4)$$

where $A_n(t)$ and $B_n(t)$ are the amplitudes.

Equations of motion: In order to derive the equations of motion for a plume parcel, we follow an analogy with the Malkus waterwheel [10, 11], a mechanical system whose rotation may also exhibit reversals with no particular regularity. On the basis of this analogy, our intent is to acquire an understanding of the wind dynamics through nonlinear model equations.

To begin, let us consider the balance of forces on the plume parcel:

$$\rho_0 \frac{dU}{dt} = f_b(\varphi, t) \sin \varphi - f_d. \quad (5)$$

Substituting the previous relations into (5), and integrating the resultant expression with respect to φ from 0 to 2π , one readily finds:

$$\frac{dU}{dt} = \frac{1}{2} \alpha_p g A_1 - \frac{3}{8} C_\varepsilon(\text{Re}) \frac{U^2}{\ell}. \quad (6)$$

Remarkably, the temporal behavior of U is coupled to the amplitude of the first temperature mode A_1 only.

Concerning the temperature variations, we write:

$$\frac{\partial T}{\partial t} + \frac{2U}{L} \frac{\partial T}{\partial \varphi} = \kappa \frac{(T_s - T)}{\ell^2}, \quad (7)$$

where the thermal loss of the plume parcel is taken as proportional to the difference between its temperature T and the temperature T_s of its surrounding, i.e., the term $\kappa \nabla^2 T$ is modeled by $\kappa(T_s - T)/\ell^2$. Substituting (3) and (4) into (7), and equating the coefficients of each harmonic separately, one obtains

$$\frac{dA_1}{dt} = -\frac{\kappa}{\ell^2} A_1 + \frac{2}{L} U B_1, \quad (8)$$

$$\frac{dB_1}{dt} = -\frac{\kappa}{\ell^2} B_1 + \frac{\kappa \Delta}{2\ell^2} - \frac{2}{L} U A_1. \quad (9)$$

It is convenient to write the three coupled ODEs (6), (8), and (9) in nondimensional form. We introduce the dimensionless size γ of the plume parcel as $\gamma = \ell/L$

and the dimensionless variables as $\tau = \kappa L^{-2} \gamma^{-2} t$, $Y = 2r\Delta^{-1} A_1$, $X = 2\gamma^2 L \kappa^{-1} U$, and $Z = -(1+2B_1\Delta^{-1})r$, where the control parameters are given by

$$\sigma = \left(\frac{9}{4}\right)^{\frac{3}{2}} \gamma(\text{Ra}, \text{Pr}) \text{Pr}, \quad (10)$$

$$r = \frac{1}{2} \left(\frac{4}{9}\right)^{\frac{3}{2}} [\gamma(\text{Ra}, \text{Pr})]^3 \text{Ra}. \quad (11)$$

Thus, the system of equations (6), (8) and (9) becomes

$$\frac{dX}{d\tau} = \sigma Y - \sigma X - X \left[\sigma^2 + \left(\frac{\beta \text{Pr}}{\sigma} \right)^2 X^2 \right]^{1/2} \quad (12)$$

$$\frac{dY}{d\tau} = r X - Y - X Z, \quad (13)$$

$$\frac{dZ}{d\tau} = -Z + X Y, \quad (14)$$

where $\beta = \frac{3}{16} \left(\frac{27}{2k}\right)^{3/2}$. Such system resembles the structure of the Lorenz equations [12, 13], which have also been used to describe *laminar* flow confined in a toroidal loop [14, 15]. It should be noted that here Eqs. (12)-(14) have been derived for plume reversals in the *turbulent* regime. They will be referred to as the *modified* Lorenz equations. Indeed, there are three essential differences with respect to the standard Lorenz system [16, 17]:

1. The parameters σ and r depend on Re , namely $\sigma \sim \text{Pr} \text{Re}^{-3/4}$ and $r \sim \text{Ra} \text{Re}^{-9/4}$. This is a key difference, since in the Lorenz equations $\sigma = \text{Pr}$ and $r \sim \text{Ra}$.
2. The ordinary differential equation for X has a *new* nonlinear term, due to the turbulent drag on the plume parcel.
3. The Lorenz system is invariant under the transformation $X \rightarrow -X$ and $Y \rightarrow -Y$, which is not the case for the modified equations. Due to the new nonlinear term the symmetry of the velocity equation is broken. Such symmetry breaking is expected in the turbulent regime.

Phase diagram: To investigate whether the dynamical system (12)-(14) captures the reversal mechanism, we have numerically scanned a region of the parameter space $\text{Pr} \times \text{Ra}$, with $3 \leq \text{Pr} \leq 1000$ and $10^7 \leq \text{Ra} \leq 10^{14}$. The integration process has been performed using the initial condition $(X = 0, Y = 1, Z = 0)$ and the $\text{Re}(\text{Ra}, \text{Pr})$ input from Grossmann-Lohse theory [18], with increments of 0.1 for $\log_{10}(\text{Pr})$, and 0.25 for $\log_{10}(\text{Ra})$.

In order to have an insight into the basic structure of the phase diagram, it is convenient to look at some representative times series of X . For $\text{Pr} = 5$, figure 2(a) shows chaotic reversals at $\text{Ra} = 10^{8.5}$, and figure 2(b) shows a uniform circulation at $\text{Ra} = 10^{11.25}$. On the

other hand, for higher Pr at a higher Ra , e.g. $\text{Pr} = 316$ at $\text{Ra} = 10^{13.25}$, periodic reversals may also emerge, as shown in figure 2(c).

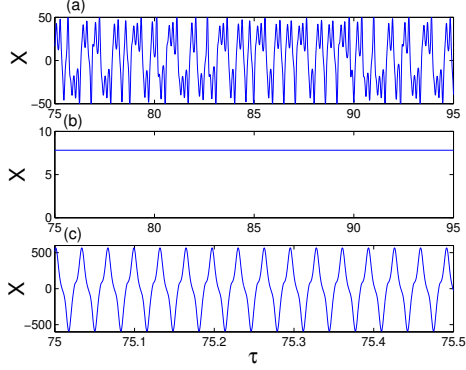


FIG. 2: Time series for $\text{Pr} = 5$ at (a) $\text{Ra} = 10^{8.5}$ (chaotic reversals) and (b) $\text{Ra} = 10^{11.25}$ (stable wind). In (c), periodic reversals are exhibited for $\text{Pr} = 316$ at $\text{Ra} = 10^{13.25}$.

In figure 3, a schematic picture of the phase diagram is presented. Roughly speaking, there are 3 regimes of interest: (i) the regime of no circulation, (ii) the reversal regime, in which the wind switches its direction chaotically or periodically; and (iii) the regime of uniform circulation, in which (after transient effects) the parcel circulates with constant speed. Additional computations performed with different initial conditions suggest that this basic structure of the phase diagram (namely, a diagonal region corresponding to chaotic reversals) does not change significantly.

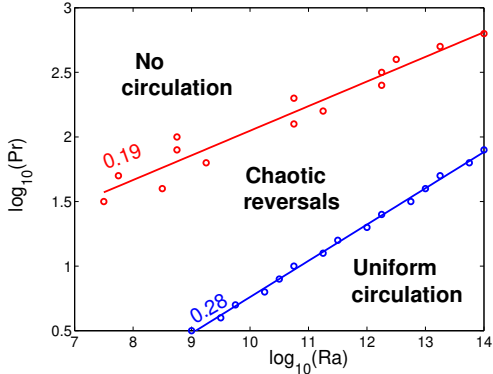


FIG. 3: Phase diagram in the $\text{Pr} \times \text{Ra}$ plane: The upper solid line represents the onset of reversals, and the lower solid line demarcates the transition to the regime of uniform circulation. The diagonal region consists of a chaotic sea.

In spite of the artifacts generated by the model (e.g. small periodic islands within the chaotic sea), it is still interesting to investigate the physical basis of the onset of reversals, and the transition to the regime of uniform circulation. Next we address these issues.

Transitions in the phase diagram: The onset of reversals can be understood in terms of the typical time scales of the system, namely: the turnover time $\tau_U = \pi L/U$, and the thermal diffusion time $\tau_\kappa = \ell^2/\kappa$. Qualitatively, it is reasonable to expect wind reversals when $\tau_U \ll \tau_\kappa$, because in such circumstance the circulation is so fast that the plume parcel has no time to lose temperature contrast. In fact, invoking equation (2) one readily obtains that the ratio τ_U/τ_κ is given by:

$$\frac{\tau_U}{\tau_\kappa} = \frac{\pi \sqrt{C_\epsilon(\text{Re})}}{100} \text{Pr}^{-1} \text{Re}^{1/2}. \quad (15)$$

Numerically, constant ratios $\tau_U/\tau_\kappa = a_0$ define a family of lines with effective slope 0.16 (close to 0.19 obtained from the fit in figure 3). In particular, the upper transition line in figure 3 can be associated with $a_0 \simeq 0.73$. Physically, this means that when $\tau_U < 0.73 \tau_\kappa$, the plume parcel is too fast to cool down within half a turnover, and hence reversals occur. This analysis reveals that two regions in the phase diagram should be distinguished: (i) the region above the onset line, where $\tau_U/\tau_\kappa < a_0$, and (ii) the region below the onset line, where $\tau_U/\tau_\kappa > a_0$.

The lower region exhibits an additional type of transition: when $\tau_U/\tau_\kappa \gg a_0$, a *single* plume parcel is so small (since ℓ decreases with increasing Ra) that its temperature rapidly gets coupled to the temperature of its surrounding. Thus, the interplay between buoyancy and drag may result in a uniform circulation. According to equation (6), the buoyancy force is determined by the temperature mode A_1 , which can be interpreted as the typical temperature of the plume parcel with respect to its surrounding. In the regime of uniform circulation $dU/dt = 0$, equation (6) leads to:

$$\frac{A_1}{\Delta} = \frac{3}{40} [C_\epsilon(\text{Re})]^{5/4} \text{Pr} \text{Ra}^{-1} \text{Re}^{11/4}.$$

Similarly as in the previous analysis, constant ratios $A_1/\Delta = a_1$ define a family of lines with effective slope 0.26. In particular, the lower transition line in figure 3 can be associated with $a_1 \simeq 0.006$. Physically, this suggests that when $A_1 < 0.006\Delta$, the buoyancy force on a *single* plume parcel is not enough to counteract the circulation.

Reynolds number: We now come to the dependence of the Reynolds number $\text{Re}_{rms} = L u_{rms} \nu^{-1}$ based on the root mean square velocity $u_{rms} = \sqrt{\langle (U - \langle U \rangle)^2 \rangle}$, where $\langle \cdot \rangle$ denotes a time average. Figure 4 shows that $\text{Re}_{rms} \sim \text{Pr}^{-(0.80 \pm 0.01)} \text{Ra}^{0.43 \pm 0.01}$. This scaling is in reasonable agreement with the experimental measurements by Xia et al. [19] $\text{Re}_{rms} \sim \text{Pr}^{-(0.86 \pm 0.01)} \text{Ra}^{0.40 \pm 0.03}$.

Mean reversal frequency: The abrupt character of reversals [cf. figure 2(a)] suggests that a wind switching can be considered as an instantaneous event represented by the moment at which it occurs. Thus, we will follow Sreenivasan et al. [4] and define t'_n as the interval

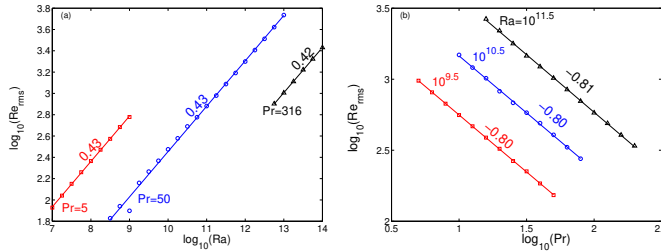


FIG. 4: Reynolds number Re_{rms} based on the root mean square velocity as function of (a) Ra and (b) Pr .

between an arbitrary origin in time and the n th wind reversal. Similarly as in [4], we also find a linear relation $t'_n \sim n$, which suggests that a mean interval between reversals can be defined. Denoting the slope of the (fitted) line by \bar{t}' , we define $\omega = 1/\bar{t}'$ as the mean reversal frequency.

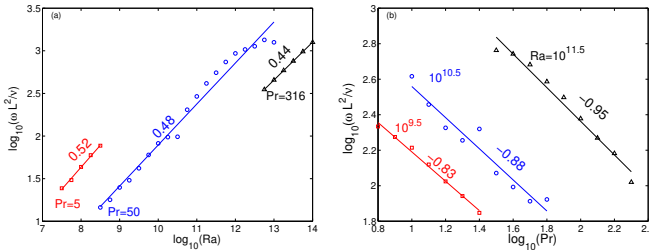


FIG. 5: Mean reversal frequency as function of (a) Ra and (b) Pr .

Figure 5 shows the dependence of the dimensionless frequency $\tilde{\omega} = \omega L^2/\nu$ on Ra and Pr . For falling (fixed) Pr from 316 to 5 the effective Ra -scaling exponent of $\tilde{\omega}$ increases from 0.44 to 0.52. The recent experimental result [20] for the wind reversal frequency in cryogenic helium gas ($Pr = 0.75$) $\tilde{\omega} \sim Ra^{0.71}$ (for $2.1 \times 10^8 \leq Ra \leq 1 \times 10^{13}$) would fit into this trend of an increasing Ra -scaling exponent with decreasing Pr . Note, however, that our model for a *single* plume does not exhibit reversals for $Pr < 1$ at $Ra > 10^6$, and such limitation does not allow us to make a quantitative comparison with this particular experiment [20]. – For fixed Ra between $10^{9.5}$ and $10^{11.5}$ the model predicts an effective Pr -scaling exponent of the reversal frequency $\tilde{\omega}$ between -0.83 and -0.95 ; a prediction which should be tested in experiment.

In summary, our model reveals the mechanism of wind reversal. It is remarkable how many features of our force

and temperature balance model agree with experimental observations for the wind reversal and that even predictions are possible. In future work plume-plume interaction has to be included into the model. Preliminary results show that the large Ra regime of uniform circulation then vanishes and chaotic reversals stay.

We thank K. R. Sreenivasan and J. Niemela for fruitful exchange. This work is part of the research programme of the Stichting voor Fundamenteel Onderzoek der Materie (FOM), which is financially supported by the Nederlandse Organisatie voor Wetenschappelijk Onderzoek (NWO).

- [1] R. Krishnamurti, L. N. Howard, Proc. Natl. Acad. Sci. USA **78**, 1981-1985 (1981).
- [2] H. D. Xi, S. Lam, K. Q. Xia, J. Fluid Mech. **503**, 47-56 (2004).
- [3] J. J. Niemela, L. Skrbek, K. R. Sreenivasan, R. J. Donnelly, J. Fluid Mech. **449**, 169-178 (2001).
- [4] K. R. Sreenivasan, A. Bershadskii, J. J. Niemela, Phys. Rev. E **65**, 056306 (2002).
- [5] E. van Doorn, B. Dhruba, K. Sreenivasan, V. Cassella, Phys. Fluids **12**, 1529-1534 (2000).
- [6] G. A. Glatzmeier, R. C. Coe, L. Hongre, P. H. Roberts, Nature **401**, 885-890 (1999).
- [7] S. Grossmann, D. Lohse, *Rayleigh-Prandtl number dependent phase diagram for strong thermal convection*, in High Rayleigh Number Convection, International Workshop, September 3-5, 2001, Ilmenau, Germany.
- [8] H. Effinger, S. Grossmann, Z. Phys. B **66**, 289-304 (1987).
- [9] D. Lohse, Phys. Rev. Lett. **73**, 3223 (1994).
- [10] S. H. Strogatz, *Nonlinear dynamics and chaos*, Perseus Books, Reading (1994).
- [11] M. Kolár, G. Gumbs, Phys. Rev. A **45**, 626-637 (1992).
- [12] E. N. Lorenz, J. Atmos. Sci. **20**, 130-141 (1963).
- [13] J. B. McLaughlin, P. C. Martin, Phys. Rev. A **12**, 186-203 (1975).
- [14] M. Gorman, P. J. Widmann, Phys. Rev. Lett. **52**, 2241-2244 (1984).
- [15] P. Ehrhard, U. Müller, J. Fluid Mech. **217**, 487-518 (1990).
- [16] Obviously, the nontrivial fixed points of the modified Lorenz equations are different from those of the original Lorenz equations.
- [17] What however our modified Lorenz system has in common with the original one is that it is not suited to make statements on the heat flux in the turbulent regime.
- [18] S. Grossmann, D. Lohse, J. Fluid Mech. **407**, 27-56 (2000); Phys. Rev. Lett. **86**, 3316-3319 (2001); Phys. Rev. E **66**, 016305 (2002).
- [19] S. Lam, X.D. Shang, S.Q. Zhou, K.Q. Xia, Phys. Rev. E **65**, 066306 (2002).
- [20] J. J. Niemela, K. R. Sreenivasan, private communication.